

SUBTLE SIGNATURES OF MULTIPLICITY IN LATE-TYPE DWARF SPECTRA: THE UNRESOLVED M8.5 + T5 BINARY 2MASS J03202839–0446358¹

ADAM J. BURGASSER,^{2,3} MICHAEL C. LIU,^{4,5} MICHAEL J. IRELAND,⁶ KELLE L. CRUZ,^{3,7,8} AND TRENT J. DUPUY⁴

Submitted to ApJ 4 January 2008; Accepted 3 March 2008

ABSTRACT

Evidence is presented that 2MASS J03202839–0446358, a late-type dwarf with discrepant optical (M8:) and near-infrared (L1) spectral types, is an as-yet unresolved stellar/brown dwarf binary with late-type M dwarf and T dwarf components. This conclusion is based on low-resolution, near-infrared spectroscopy that reveals a subtle but distinctive absorption feature at 1.6 μm . The feature, which is also present in the combined light spectrum of the M8.5 + T6 binary SCR 1845–6357, arises from the combination of FeH absorption from an M8.5 primary and pseudo-continuum flux from a T5 \pm 1 secondary, as ascertained from binary spectral templates constructed from empirical data. The binary templates provide a far superior match to the overall near-infrared spectral energy distribution of 2MASS J0320–0446 than any single comparison spectra. Laser guide star adaptive optics (LGS AO) imaging observations, including the first application of LGS AO aperture mask interferometry, fail to resolve a faint companion, restricting the projected separation of the system to less than 8.3 AU at the time of observation. 2MASS J0320–0446 is the second very low mass binary to be identified from unresolved, low-resolution, near-infrared spectroscopy, a technique that complements traditional high resolution imaging and spectroscopic methods.

Subject headings: stars: binaries: general — stars: fundamental parameters — stars: individual (2MASS J03202839–0446358) — stars: low mass, brown dwarfs

1. INTRODUCTION

The optical and near-infrared spectral energy distributions of very low mass stars and brown dwarfs—late-type M, L and T dwarfs—are distinctly non-blackbody. Overlapping molecular bands and strong line emission produce a rich array of spectral diagnostics for classification and characterization of physical properties. Considerable effort is now being devoted toward decrypting the spectral fingerprints of late-type dwarfs to determine masses, ages, metallicities and other fundamental parameters (e.g., Luhman & Rieke 1999; Gorlova et al. 2003; Burgasser, Burrows & Kirkpatrick 2007; Allers et al. 2007; Liu, Leggett, & Chiu 2007). In some cases, spectral peculiarities arise when an observed source is in fact an unresolved multiple system, with components of different masses, effective temperatures, and other spectral properties. While several classes of stellar multiples are recognized on the basis of their unusual spec-

tral or photometric properties (U Geminorum stars, M dwarf + white dwarf systems, etc.), identifying such cases amongst late-type dwarfs is complicated by the influence of other physical effects. Delineation of spectral peculiarities that arise purely from multiplicity as opposed to other physical effects is essential if we hope to unambiguously characterize the physical properties of the lowest luminosity stars and brown dwarfs.

Very low mass multiple systems are important in their own right, as they enable mass and occasionally radius measurements (e.g., Lane et al. 2001; Zapatero Osorio et al. 2004; Stassun et al. 2006; Liu, Dupuy & Ireland 2008), provide constraints for star/brown dwarf formation scenarios (e.g., Close et al. 2003; Allen 2007; Luhman et al. 2007a) and facilitate detailed studies of atmospheric properties (e.g., Burgasser et al. 2006b; Liu et al. 2006; Martín et al. 2006). Of the roughly 90 very low mass multiple systems currently known,⁹ the majority have been identified through high angular resolution imaging, using the *Hubble Space Telescope* (*HST*; e.g., Martín, Brandner & Basri 1999; Bouy et al. 2003; Burgasser et al. 2006b; Reid et al. 2006a), ground-based adaptive optics systems (e.g., Close et al. 2003; Chauvin et al. 2004; Siegler et al. 2003, 2005; Kraus, White & Hillenbrand 2005; Liu et al. 2006; Looper et al. 2008) and more recently aperture masking interferometry (e.g., Ireland et al. 2008; Kraus et al. 2008). However, as the vast majority of very low mass binaries have small separations (>90% have $\rho < 20$ AU; Burgasser et al. 2007b), expanding the population of known binaries to greater distances requires either finer angular sampling or the identification of systems that are unresolved. The frequency of nearby, tightly-bound binaries is also essential for a complete assessment

¹ Some of the data presented herein were obtained at the W.M. Keck Observatory, which is operated as a scientific partnership among the California Institute of Technology, the University of California, and the National Aeronautics and Space Administration. The Observatory was made possible by the generous financial support of the W.M. Keck Foundation.

² Massachusetts Institute of Technology, Kavli Institute for Astrophysics and Space Research, Building 37, Room 664B, 77 Massachusetts Avenue, Cambridge, MA 02139, USA; ajb@mit.edu

³ Visiting Astronomer at the Infrared Telescope Facility, which is operated by the University of Hawai'i under Cooperative Agreement NCC 5-538 with the National Aeronautics and Space Administration, Office of Space Science, Planetary Astronomy Program

⁴ Institute for Astronomy, University of Hawai'i, 2680 Woodlawn Drive, Honolulu, HI 96822, USA

⁵ Alfred P. Sloan Research Fellow

⁶ Division of Geological and Planetary Sciences, California Institute of Technology, Pasadena, CA 91106, USA

⁷ Division of Astronomy and Astrophysics, California Institute of Technology, Pasadena, CA 91106, USA

⁸ Spitzer Space Telescope Postdoctoral Fellow

⁹ A current list is maintained by N. Siegler at <http://www.vlmbinaries.org>.

of the overall very low mass dwarf binary fraction, since imaging studies provide only a lower limit to this fundamental statistic. Such systems are also more likely to eclipse, enabling radius measurements and fundamental tests of evolutionary models (e.g., Stassun et al. 2006). While searches for radial velocity variability via high resolution spectroscopy can be useful in this regime (e.g., Basri & Martín 1999; Kenyon et al. 2003; Basri & Reiners 2006; Blake et al. 2007; Joergens & Müller 2007), in many cases very low luminosity and/or distant late-type dwarfs are simply too faint to be followed up in this manner.

Recently, Burgasser (2007c) demonstrated that in certain cases the presence of an unresolved companion can be inferred directly from the morphology of a source’s low-resolution near-infrared spectrum. In particular, it was shown that the spectrum of the peculiar L dwarf SDSS J080531.84+481233.0 (hereafter SDSS J0805+4812; Hawley et al. 2002; Knapp et al. 2004), which has highly discrepant optical and near-infrared spectral classifications, could be accurately reproduced as a combination of “normal” L4.5 + T5 components. Indeed, the binary hypothesis provides a far simpler and more consistent explanation for the unusual optical, near-infrared and mid-infrared properties of SDSS J0805+4812 than other alternatives (e.g., Knapp et al. 2004; Folkes et al. 2007; Leggett et al. 2007). The identification of unresolved multiples like SDSS J0805+4812 by low-resolution near-infrared spectroscopy is a potential boon for low-mass multiplicity studies, as this method is not subject to the same physical or projected separation limitations inherent to high-resolution imaging and spectroscopic techniques.

This article reports the discovery of a second unresolved very low mass binary system, 2MASS J03202839–0446358 (hereafter 2MASS J0320–0446), identified by the morphology of its low-resolution, near-infrared spectrum. The spectroscopic observations leading to this conclusion are described in § 2, as are laser guide star adaptive optics (LGS AO) imaging observations aimed at searching for a faint companion. Analysis of the spectral data using the binary template matching technique described in Burgasser (2007c) is presented in § 3. § 4 discusses the viability of 2MASS J0320–0446 being a binary, with specific comparison to the known M dwarf + T dwarf system SCR 1845–6357. We also constrain the projected separation of the 2MASS J0320–0446 system based on our imaging observations, and discuss overall limitations on the variety of unresolved M dwarf + T dwarf binaries that can be identified from composite near-infrared spectroscopy. Conclusions are summarized in § 5.

2. OBSERVATIONS

2.1. Previous Observations of 2MASS J0320–0446

2MASS J0320–0446 was originally discovered by Cruz et al. (2003) and Wilson et al. (2003) in the Two Micron All Sky Survey (2MASS; Skrutskie et al. 2006), and classified M8: (uncertain) and L0.5 on the basis of optical and near-infrared spectroscopy, respectively. The M8: optical classification is uncertain because of the low signal-to-noise of the spectral data, and is not due to any specific spectral peculiarity. Cruz et al. (2003) esti-

mate a distance of 26 ± 4 pc for this source based on its classification and empirical M_J /spectral type relations. Deacon, Hambly & Cooke (2005), using *I*-band plate data from the SuperCosmos Sky Survey (SSS; Hambly et al. 2001a,b,c), report a relatively high proper motion of $0''.68\pm 0''.04$ yr⁻¹ at position angle 191° for this source. Figure 1 shows the field around 2MASS J0320–0446 imaged by *R* and *I* photographic plates. A faint source is seen in the 1955 Palomar Sky Survey I (Abell 1959) *R*-band image roughly at the offset position indicated by the Deacon, Hambly & Cooke (2005) proper motion. By including this source position along with additional astrometry drawn from the SSS and 2MASS catalogs, an improved proper motion measurement of $0''.562\pm 0''.005$ yr⁻¹ at position angle $205.9\pm 0.5^\circ$ was determined. This proper motion and the estimated distance indicates a rather large tangential space velocity for 2MASS J0320–0446, $V_{tan} = 69\pm 11$ km s⁻¹, suggesting that it could be an older disk star. None of the previous studies of 2MASS J0320–0446 report the presence of a faint companion.

2.2. Near-Infrared Spectroscopy

Low resolution near-infrared spectral data for 2MASS J0320–0446 were obtained on 2007 September 16 (UT) using the SpeX spectrograph (Rayner et al. 2003) mounted on the 3m NASA Infrared Telescope Facility (IRTF). The conditions on this night were poor with patchy clouds, cirrus and average seeing ($0''.8$ at *J*-band), and 2MASS J0320–0446 was observed as a bright backup target ($J = 12.13\pm 0.03$). The $0''.5$ slit was used to obtain $0.7\text{--}2.5$ μm spectroscopy with resolution $\lambda/\Delta\lambda \approx 120$ and dispersion across the chip of $20\text{--}30$ Å pixel⁻¹. To mitigate the effects of differential refraction, the slit was aligned to the parallactic angle. Six exposures of 90 s each were obtained in an ABBA dither pattern along the slit. The A0 V star HD 18571 was observed immediately after 2MASS J0320–0446 and at a similar airmass (1.21) for flux calibration. Internal flat field and argon arc lamps were observed after both target and flux standard observations for pixel response and wavelength calibration. Data were reduced with the IDL SpeXtool package, version 3.4 (Cushing, Vacca, & Rayner 2004; Vacca et al. 2003), using standard settings. A detailed description of the reduction procedures is given in Burgasser (2007c).

The near-infrared spectrum of 2MASS J0320–0446 is shown in Figure 2, compared to equivalent data for the optical spectral standards VB 10 (M8; van Biesbroeck 1961; Kirkpatrick, Henry, & McCarthy 1991) and 2MASS J14392836+1929149 (L1, hereafter 2MASS J1439+1929; Kirkpatrick et al. 1999). Despite the poor observing conditions, the data for 2MASS J0320–0446 have exceptionally good signal-to-noise, $\gtrsim 150$ in the *JHK* flux peaks and ~ 50 in the bottom of the 1.4 and 1.8 μm H₂O bands. Color biases due to telluric cloud absorption do not appear to be present, as indicated by comparison of 2MASS photometry and synthetic *J–H*, *H–K_s* and *J–K_s* colors computed from the spectral data, which agree to within the photometric uncertainties.

The morphology of the near-infrared spectrum of 2MASS J0320–0446 is typical of a late-type M or early-type L dwarf, with bands of TiO and VO absorption at

red optical wavelengths ($\lambda < 1 \mu\text{m}$); prominent H_2O absorption at 1.4 and 1.8 μm ; FeH absorption at 0.99, 1.2 and 1.55 μm ; Na I and K I line absorption in the 1.0–1.3 μm region; weak Na I lines at 2.2 μm ; and strong CO bandheads at 2.3–2.4 μm . For the most part, the spectrum of 2MASS J0320–0446 is more consistent with that of 2MASS J1439+1929; note in particular the similarities in the overall shape of the 1.0–1.35 μm J -band flux peak and the deep 1.4 μm H_2O band. However, TiO and VO bands are more similar to (but weaker than) those seen in the spectrum of VB 10, while the weak 2.2 μm Na I lines are rarely seen in L dwarf spectra (e.g., McLean et al. 2003). The near-infrared spectrum of 2MASS J0320–0446 is also somewhat bluer than that of 2MASS J1439+1929, in line with their respective colors ($J - K_s = 1.13 \pm 0.04$ versus 1.21 ± 0.03).

The similarities to 2MASS J1439+1929 suggests an L1 near-infrared spectral type for 2MASS J0320–0446, which is confirmed by examination of the spectral indices and index/spectral type relations defined by Reid et al. (2001a) and Geballe et al. (2002). The average subtype for the four indices K1 (measuring the shape of the K -band flux peak; Tokunaga & Kobayashi 1999), $\text{H}_2\text{O-A}$, $\text{H}_2\text{O-B}$ and $\text{H}_2\text{O-1.5}$ (all measuring the strength of the 1.4 μm H_2O band) yields a near-infrared classification of L1 (± 0.6 subtypes), consistent with the L0.5 near-infrared classification reported by Wilson et al. (2003).

This classification is fully three subtypes later than the M8: optical spectral type reported by Cruz et al. (2003). However, such discrepancies are not altogether uncommon amongst late-type dwarfs. Geballe et al. (2002) and Knapp et al. (2004) have found disagreements of up to 1.5 subtypes between optical (based on the Kirkpatrick et al. 1999 scheme) and near-infrared classifications (based on their own scheme) for several L dwarfs. Burgasser et al. (2008) have discussed a subclass of unusually blue L dwarfs whose optical classifications are consistently 2–3 subtypes earlier than their near-infrared classifications. Such discrepancies have been variously attributed to surface gravity, metallicity, condensate cloud or multiplicity effects (e.g., Knapp et al. 2004; Chiu et al. 2006; Cruz et al. 2007; Folkes et al. 2007; Burgasser et al. 2008). The large V_{tan} of 2MASS J0320–0446, indicating that this source may be somewhat older, suggests that high surface gravity and/or slightly subsolar metallicity could explain the discrepant optical and near-infrared spectral classifications.

However, 2MASS J0320–0446 exhibits one unusual feature not seen in the comparison spectra in Figure 2, a slight dip at 1.6 μm , that suggests multiplicity is relevant in this case. The 1.6 μm feature is nearly coincident with the 1.57–1.64 μm FeH absorption band commonly observed in L dwarf near-infrared spectra (Wallace & Hinkle 2001; Cushing et al. 2003). Yet its morphology is clearly different, with a cup-shaped depression as opposed to the flat plateau seen in the comparison spectra of Figure 2. More importantly, this feature has the same morphology and is centered at the same wavelength as the peculiar feature noted in the spectrum of SDSS J0805+4812 (Burgasser 2007c). In that case, the 1.6 μm feature and other spectral peculiarities were attributed to the presence of a mid-type T dwarf companion. Given the similar discrepancy in optical and near-infrared classifications for SDSS J0805+4812 (L4 and

L9.5, respectively), it is reasonable to consider whether 2MASS J0320–0446 also harbors a faint T dwarf companion.

2.3. High Angular Resolution Imaging

In an attempt to search for faint companions, 2MASS J0320–0446 was imaged on 2008 January 15 (UT) with the sodium LGS AO system (Wizinowich et al. 2006; van Dam et al. 2006) and facility near-infrared camera NIRC2 on the 10m Keck Telescope. Conditions were photometric with average/below-average seeing. The narrow field-of-view camera of NIRC2 was utilized, providing an image scale of 9.963 ± 0.011 mas/pixel (Pravdo et al. 2006) over a $10.2'' \times 10.2''$ field of view. All observations were conducted using the MKO¹⁰ K_s -band filter. The LGS provided the wavefront reference source for AO correction, while tip-tilt aberrations and quasi-static changes were measured contemporaneously by monitoring the $R = 16.7$ mag field star USNO-B1.0 0852–0031783 (Monet et al. 2003), located $14''$ away from 2MASS J0320–0446. The LGS, with an equivalent brightness of a $V \approx 10.4$ mag star, was pointed at the center of the NIRC2 field-of-view for all observations.

2MASS J0320–0446 was imaged using two different methods in order to probe the widest possible range of projected separations: (1) direct imaging and (2) aperture mask interferometry. In the first case, a series of 3 dithered 60-second images was obtained, offsetting the telescope by a few arcseconds between exposures, for a total integration time of 180 seconds. Raw frames were reduced using standard procedures. Normalized flat field frames were constructed from the differences of images of the telescope dome interior with and without continuum lamp illumination. A master sky frame was created from the median average of the bias-subtracted, flat-fielded images and subtracted from the individual exposures. Individual frames were registered and stacked to form a final mosaic imaged. The observations achieved a point spread function (PSF) full-width at half-maximum of $0''.07$ and a Strehl ratio of 0.21. With the exception of the primary target, no sources were detected in a $6'' \times 6''$ region centered on 2MASS J0320–0446.

Aperture mask observations were also obtained with the LGS AO+NIRC2 instrumental setup. In this method, a 9-hole aperture mask is placed in a filter wheel near a re-imaged pupil plane within the NIRC2 camera. The mask has non-redundant spacing, so each Fourier component of the recorded image corresponds to a unique pair of patches on the Keck primary mirror. The primary interferometric observables of squared visibility and closure-phase are therefore calibrated much better than images using the full aperture. This technique has a long history of achieving the full diffraction limit of a telescope (e.g. Michelson 1920; Baldwin et al. 1986; Nakajima et al. 1989; Tuthill et al. 2000) and has been recently applied to natural guide star AO observations at Keck (Ireland et al. 2008; Kraus et al. 2008). This is the first application of aperture mask interferometry to LGS AO observations that we are aware of.

2MASS J0320–0446 was observed in this setup us-

¹⁰ Mauna Kea Observatory (MKO) photometric system; Simons & Tokunaga (2002); Tokunaga, Simons & Vacca (2002).

ing a two-point dither pattern, with five 50-second integrations at each dither position. The nearby field star 2MASS J03381363–0332508, which has a similar K_s -band brightness and tip-tilt star asterism as 2MASS J0320–0446, was contemporaneously observed to calibrate both instrumental closure phase and visibility. Images of the interferograms formed by the mask were recorded by the NIRC2 detector, and squared visibilities and closure-phases were extracted from the image Fourier transforms. Raw visibility amplitudes were ~ 0.05 on the longest baselines. The closure phases for this calibrator star were subtracted from those of 2MASS J0320–0446, while the calibrator’s squared visibilities were divided into those of 2MASS J0320–0446. The one-sigma scatter in the calibrated closure phase was 5° . Using standard analysis techniques (e.g., Kraus et al. 2008), we found no evidence of a binary solution in the data.

Upper limits on the presence of a faint companion to 2MASS J0320–0446 were computed separately for the direct imaging and aperture mask observations. For the direct imaging data, upper limits were determined by first smoothing the final mosaic with an analytical representation of the PSF’s radial profile, modeled as the sum of multiple gaussians. We then measured the standard deviation of flux counts in concentric annuli out to $3''$ in radius centered on the science target, normalized by the peak flux of the science target. We considered $10\times$ these values as the flux ratio limits for any companions, as visually verified by inserting fake sources into the image using translated and scaled versions of the science target. For the aperture mask data, detection limits at 99% confidence were calculated in three annuli spanning $0''.020$ – $0''.16$ in separation (the lower limit corresponding to the diffraction limit of the aperture mask) using the Monte-Carlo approach described in Kraus et al. (2008).

Figure 3 displays the resulting flux ratio limits for a faint companion as a function of separation for both datasets. At separations $\lesssim 0''.25$, the aperture mask data exclude any companions with $\Delta K_s \lesssim 3$ mag for separations down to $0''.04$. Note that better seeing, as opposed to longer integrations, would have provided greater improvement in sensitivity in this range. The direct imaging observations exclude any companions with $\Delta K_s \lesssim 7$ mag at separations $\gtrsim 0''.7$, with the floor set primarily by sky shot noise and detector read noise. These limits are discussed further in § 4.1.

3. BINARY TEMPLATE MATCHING

3.1. Spectral Sample

As an alternative method to identify and characterize a possible companion to 2MASS J0320–0446, a variant of the binary spectral template matching technique described in Burgasser (2007c) was applied to the near-infrared spectral data.¹¹ In this method, the spectrum of a late-type source is compared to a large set of binary spectral templates constructed from empirical data for M, L and T dwarfs. The component spectra of each binary template were scaled according to empirical absolute magnitude/spectral type relations. To minimize

systematic effects, source and template spectra are required to have the same resolution and wavelength coverage, which is facilitated in this case by using a sample of nearly 200 SpeX prism spectra of M5–T8 dwarfs drawn from the literature¹² and our own unpublished observations. Spectral types for the sources in this sample were assigned according to published classifications,¹³ based either on the optical classification schemes of Kirkpatrick, Henry, & McCarthy (1991) and Kirkpatrick et al. (1999) for M5–L8 dwarfs or the near-infrared classification scheme of Burgasser et al. (2006a) for L9–T8 dwarfs (M and L dwarfs with only near-infrared classifications reported were not included here). The initial spectral sample was purged of low signal-to-noise data as well as spectra of those sources known to be binary or noted as peculiar in the literature (e.g., low surface gravity brown dwarfs, subdwarfs, etc.). This left a sample of 132 spectra of 125 sources, listed in Table 1.

3.2. Single Template Fits

To ascertain whether an unresolved binary truly provides a better fit to the spectrum of 2MASS J0320–0446, comparisons were first made to individual sources in the SpeX sample. All spectra were initially normalized to their peak flux in the 1.2 – $1.3 \mu\text{m}$ band. The statistic σ^2 was then computed between the 2MASS J0320–0446 ($f_\lambda(0320)$) and template spectra ($f_\lambda(T)$), where

$$\sigma^2 \equiv \sum_{\{\lambda\}} \frac{[f_\lambda(0320) - f_\lambda(T)]^2}{f_\lambda(0320)} \quad (1)$$

(see Burgasser 2007c). The summation is performed over the wavelength ranges $\{\lambda\} = 0.95$ – $1.35 \mu\text{m}$, 1.45 – $1.8 \mu\text{m}$ and 2.0 – $2.35 \mu\text{m}$ in order to avoid regions of strong telluric absorption. The denominator provides a rough estimate of shot noise in the spectral data, which is dominant in the highest signal-to-noise spectra, and therefore makes σ^2 a rough approximation of the χ^2 statistic.¹⁴ To eliminate normalization biases, each template spectrum was additionally scaled by a multiplicative factor in the range 0.5 – 1.5 to minimize σ^2 .

Figure 4 displays the four best single template matches, all having $\sigma^2 < 0.6$. The three best-fitting sources—LEHPM 1-6333 (M8), 2MASS J1124+3808 (M8.5) and LEHPM 1-6443 (M8.5)—have optical spectral types consistent with the optical type of 2MASS J0320–0446. The fourth-best fit, the L1 2MASS J1493+1929, was shown to provide an adequate match to the spectrum of 2MASS J0320–0446 in Figure 2. The LEHPM¹⁵

¹² See Burgasser et al. (2004, 2006a, 2007a); Cruz et al. (2004); Siegler et al. (2005); Burgasser, Burrows & Kirkpatrick (2007); Burgasser & McElwain (2006); Chiu et al. (2006); McElwain & Burgasser (2006); Reid et al. (2006b); Burgasser (2007a,b); Liebert & Burgasser (2007);Looper, Kirkpatrick & Burgasser (2007); and Luhman et al. (2007b). These data are available at <http://www.browndwarfs.org/spexprism>.

¹³ A current list of L and T dwarfs with their published optical and near-infrared spectral types is maintained by C. Gelino, J. D. Kirkpatrick and A. Burgasser at <http://www.dwarfarchives.org>.

¹⁴ In the near-infrared, foreground emission generally dominates noise contributions. However, given the broad range of observing conditions in which the 2MASS J0320–0446 and template data were taken, we chose not to include this term in our σ^2 statistic.

¹⁵ Liverpool-Edinburgh High Proper Motion (LEHPM) Catalog of Pokorny et al. (2004).

¹¹ See also Burgasser et al. (2005, 2006b, 2008); Reid et al. (2006b); Burgasser (2007b);Looper, Kirkpatrick & Burgasser (2007); Siegler et al. (2007); and Looper et al. (2008).

sources have large proper motions ($\mu > 0''.4 \text{ yr}^{-1}$), notably similar to 2MASS J0320–0446. All four sources shown in Figure 4 provide reasonably good matches to the broad near-infrared spectral energy distribution of 2MASS J0320–0446, but with two key discrepancies: an absence of the $1.6 \mu\text{m}$ feature (inset boxes in Figure 4) and a shortfall in the peak spectral flux at $1.27 \mu\text{m}$. In the first case, FeH absorption bands are clearly seen in the comparison spectra but do not produce the distinct dip seen in the spectrum of 2MASS J0320–0446. In the second case, the spectrum of 2MASS J0320–0446 is consistently brighter in the $1.2\text{--}1.35 \mu\text{m}$ range as compared to the (appropriately scaled) late-type M dwarf templates. As demonstrated below, both of these discrepancies can be resolved by the addition of a T dwarf component.

3.3. Binary Template Fits

Binary spectral templates from the SpeX prism sample were constructed by first flux-calibrating each spectrum according to established absolute magnitude/spectral type relations. For M5–L5 dwarfs, the 2MASS M_J /spectral type relation of Cruz et al. (2003) was used. For L5–T8 dwarfs, both of the MKO M_K /spectral type relations defined in Liu et al. (2006) were considered. The Liu et al. relations are based on a sample of L and T dwarfs with measured parallaxes and MKO photometry, but one relation (“bright”) was constructed after rejecting known (resolved) binaries while the other relation (“faint”) was constructed after rejecting all known and *candidate* binaries as described in that study. As illustrated in Figure 3 of Burgasser (2007b), these two relations envelope the M_K values of currently measured sources (including components of resolved binaries), but diverge by as much as ~ 1 mag for spectral types L8–T5. Nevertheless, the Liu et al. (2006) relations represent our current best constraints on the absolute magnitude/spectral type relation across the L dwarf/T dwarf transition. In all cases, synthetic magnitudes to scale the data were calculated directly from the spectra. Binary templates were then constructed by adding together the calibrated spectra of source pairs whose types differ by at least 0.5 subclasses, producing a total of 8248 unique combinations. The binary templates were then normalized to their peak flux in the $1.2\text{--}1.3 \mu\text{m}$ band and compared to the spectrum of 2MASS J0320–0446 in the same manner as the single source templates; i.e., with additional scaling to minimize σ^2 .

Figure 5 displays the best fitting binary templates constructed from the primaries shown in Figure 4 and using the “faint” M_K /spectral type relation of Liu et al. (2006). For all four cases, the addition of a mid-type T dwarf secondary spectrum considerably improves the spectral template match. In particular, the $1.6 \mu\text{m}$ spectral dip is very well reproduced, while the flux peaks at $1.27 \mu\text{m}$ in the binary templates are more consistent with the spectrum of 2MASS J0320–0446. Even detailed alkali line and FeH features in the $0.9\text{--}1.3 \mu\text{m}$ region are better matched with the binary templates.

Figure 6 displays the best fitting binary templates using the “bright” M_K /spectral type relation of Liu et al. (2006). There is a small degree of improvement in these fits over those using the “faint” M_K relation, although the differences are very subtle due to the very small con-

tribution of light by the T dwarf secondaries ($\Delta J \approx 3.5$ mag, depending on the components). This result is fortuitous, as it indicates that the better fits provided by the binary templates are only weakly dependent on the absolute magnitude relation assumed over a spectral type range in which such relations are currently most uncertain.

Besides the best-fit comparisons shown in Figures 5 and 6, there were many excellent matches ($\sigma^2 < 0.1$) found among binaries templates which had LEHPM 1-6333 or 2MASS J1124+3808 as primaries: 30 for the “faint” M_K /spectral type relation and 58 for the “bright” relation. The average primary and secondary spectral types for the combinations in this well-matched sample are $M8.5 \pm 0.3$ and $T5.0 \pm 0.9$, respectively, with no significant differences between analyses using the “faint” or “bright” M_K /spectral type relations. The mean relative magnitudes of the primary and secondary components were $\Delta J = 3.5 \pm 0.2$ mag, $\Delta H = 4.3 \pm 0.3$ mag, $\Delta K = 4.9 \pm 0.3$ mag for the “faint” relation and $\Delta J = 3.1 \pm 0.4$ mag, $\Delta H = 3.8 \pm 0.5$ mag, $\Delta K = 4.3 \pm 0.6$ mag for the “bright” relation, as calculated directly from the flux-calibrated spectral templates. There is a large difference in the relative magnitudes between these two relations. If resolved photometry is eventually obtained for this system, such measurements could provide a means of distinguishing which of the absolute magnitude relations proposed in Liu et al. (2006) accurately characterize mid-type T dwarfs.

The origin of the $1.6 \mu\text{m}$ feature in the spectrum of 2MASS J0320–0446 is clearly revealed in Figures 5 and 6: it is a combination of FeH absorption in the M dwarf primary and CH_4 absorption in the T dwarf secondary. Specifically, the relatively sharp H -band flux peak in the spectrum of the T dwarf secondary blueward of the $1.6 \mu\text{m}$ CH_4 band contributes light to the $1.55\text{--}1.6 \mu\text{m}$ spectrum of the composite system. This is on the blue end of the $1.55\text{--}1.65 \mu\text{m}$ FeH absorption band, producing a distinct “dip” feature. Similarly, the apparently brighter $1.2\text{--}1.35 \mu\text{m}$ flux in the spectrum of 2MASS J0320–0446 can be attributed to the T dwarf companion, which exhibits a narrow J -band peak between strong $1.1 \mu\text{m}$ and $1.4 \mu\text{m}$ H_2O and CH_4 bands. Both spectral features are therefore unique to binaries containing late-type M and L dwarf primaries (in which FeH is prominent) and T dwarf secondaries.

4. DISCUSSION

4.1. Is 2MASS J0320–0446 an M dwarf plus T dwarf Binary?

It may be concluded from the analysis above that the near-infrared spectrum of 2MASS J0320–0446, and in particular the subtle feature observed at $1.6 \mu\text{m}$, can be accurately reproduced by assuming that this source is an unresolved $M8.5 + T5$ binary. But does this mean that 2MASS J0320–0446 actually is a binary? Our LGS AO imaging observations failed to detect any faint secondaries near 2MASS J0320–0446 to the limits displayed in Figure 3. Based on the “bright” MKO M_K /spectral type relation of Liu et al. (2006) and the K_s/K filter transformations of Stephens & Leggett (2004), the measured upper limits rule out a T5 companion wider than a projected separation of $\sim 0''.33$, or roughly 8.3 AU at the estimated distance of 2MASS J0320–0446 (see below).

This is a relatively weak constraint given that less than 25% of known very low mass binaries have projected separations at least this wide (Burgasser et al. 2007b). Furthermore, 2MASS J0320–0446 could have been observed in an unfortunate geometry, as was originally the case for the L dwarf binary Kelu 1 (Martín, Brandner & Basri 1999; Liu & Leggett 2005; Gelino, Kulkarni & Stephens 2006). On the other hand, if the physical separation of the 2MASS J0320–0446 system is significantly smaller than indicated by the imaging observations, high resolution spectroscopic monitoring could potentially reveal radial velocity signatures, although this depends critically on the component masses of this system. Indeed, the determination of a spectroscopic orbit in combination with the component spectral types deduced here would provide both mass and age constraints for this system, making it a potentially powerful benchmark test for evolutionary models.

An alternative test of the binary hypothesis for 2MASS J0320–0446 is to identify similar spectral traits in a comparable binary system. Fortunately, one such system is known: the M8.5 + T6 binary SCR 1845–6357 (Hambly et al. 2004; Biller et al. 2006; Montagnier et al. 2006). This nearby (3.85 ± 0.02 pc; Henry et al. 2006), well-resolved binary (angular separation of $1''.1$) has individually classified components based on resolved spectroscopy (Kasper et al. 2007). More importantly, the relative near-infrared magnitudes of this system ($\Delta J = 3.68 \pm 0.03$ mag, $\Delta H = 4.20 \pm 0.04$ mag, $\Delta K = 5.12 \pm 0.03$ mag; Kasper et al. 2007) are somewhat larger than but consistent with the estimated relative magnitudes of the putative 2MASS J0320–0446 system. Figure 7 displays the component spectra of this system, scaled to their relative H -band magnitudes,¹⁶ as well as the sum of the component spectra. The composite spectrum shows a relative increase in spectral flux as compared to the primary in both the 1.2 – 1.35 μm and 1.55 – 1.6 μm regions. Indeed, the latter gives rise to the same “dip” feature observed in the H -band spectrum of 2MASS J0320–0446, particularly when the SCR 1845–6357AB data are reduced in resolution to match that of the SpeX prism data (inset box in Figure 7). The presence of this feature in the composite spectrum of a known M dwarf plus T dwarf binary lends some confidence to the conclusion that 2MASS J0320–0446 is itself an M dwarf plus T dwarf binary.

Assuming then that 2MASS J0320–0446 is a system with M8.5 and T5 dwarf components, it is possible to characterize the physical properties of these components in some detail based on the analysis in § 3.3. Synthetic component JHK magnitudes on the MKO system as-

¹⁶ The J -band portion of the spectrum of SCR 1845–6357A shown here is slightly reduced relative to the H - and K_s -band spectra as shown to Figure 2 in Kasper et al. (2007). The relative flux calibration between spectral orders applied in that study did not account for missing data over 1.33 – 1.50 μm , slightly inflating the flux levels in the J -band. A recalibration of this spectrum was made by scaling each order by a constant factor to match the SpeX prism spectrum of 2MASS J1124+3808, which has a similar $J - K_s$ color (1.14 ± 0.03 versus 1.06 ± 0.03 for SCR 1845–6357 from Kasper et al. 2007) and optical spectral type (M8.5). Such recalibration is not necessary for the SCR 1845–6357B spectrum due to the strong 1.35 μm CH₄ and 1.4 μm H₂O bands in this source. The recalibration of the SCR 1845–6357A J -band spectrum does not affect the analysis presented here, which depends solely on the relative H -band scaling of the component spectra.

suming the “bright” M_K /spectral type relation of Liu et al. (2006) were computed from the best-fitting binary templates ($\sigma^2 < 0.1$) and are listed in Table 2. The M dwarf primary is only slightly fainter than the composite source, while the T dwarf companion is exceptionally faint, $J = 16.4 \pm 0.4$ mag. The low luminosity of the secondary, $\log_{10} L_{bol}/L_{\odot} = -5.0 \pm 0.3$ dex based on its inferred spectral type (Golimowski et al. 2004; Burgasser 2007b), suggests that 2MASS J0320–0446 could have a relatively low system mass ratio ($q \equiv M_2/M_1$). However, the mass ratio depends critically on the age of the system, for which the analysis presented above provides no robust constraints. Using the evolutionary models of Burrows et al. (1997) and component luminosities as listed in Table 2, primary and secondary mass estimates for ages of 1, 5 and 10 Gyr were derived. If 2MASS J0320–0446 is an older system, as suggested by its large V_{tan} , its inferred mass ratio $q > 0.8$ is consistent with the typical mass ratios of very low mass binaries in the field (e.g., Allen 2007). Based on the primary’s photometry and spectral type, and the M_J /spectral type relation of Cruz et al. (2003), a distance of 25 ± 3 pc is estimated for the 2MASS J0320–0446 system.

4.2. On the Identification of M dwarf plus T dwarf Binaries from Composite Near-Infrared Spectra

The subtlety of the peculiar features present in the composite spectra of 2MASS J0320–0446 and SCR 1845–6357 is due entirely to the considerable difference in flux between their M and T dwarf components. Yet in both cases the 1.6 μm feature, indicating the presence of a T dwarf companion, can be discerned. But for how early of an primary can a binary with a T dwarf companion be identified in this manner, and what variety of T dwarf companions can be discerned in such systems? To examine these questions, Figure 8 displays binary spectral templates for four primary types—M7, M8, M9 and L0—combined with T0–T8 dwarf secondaries. For all cases, the 1.6 μm feature is most pronounced when the secondary is a mid-type T dwarf, spectral types T3–T5. This is due to a tradeoff in the sharpness of the H -band flux peak in this component (i.e., the strength of 1.6 μm CH₄ absorption, which deepens with later spectral types) and its brightness relative to the primary. Not surprisingly, the 1.6 μm feature is more pronounced in binaries with later-type primaries, making it a useful multiplicity diagnostic for L dwarf + T dwarf systems (such as SDSS J0805+4812) but far more subtle in systems with M dwarf primaries. Indeed, the spectra in Figure 8 suggest that this feature is basically undetectable in binaries with M7 and earlier-type primaries. 2MASS J0320–0446 and SCR 1845–6357 probably contain the earliest-type primaries for which a T dwarf secondary could be identified solely from their composite near-infrared spectra.

It is also important to consider the other prominent spectral peculiarity caused by the presence of a T dwarf companion, the slight increase in flux at 1.3 μm . This feature increases the contrast in the 1.4 μm H₂O band, and therefore serves to bias H₂O spectral indices toward later subtypes. This effect explains why the near-infrared classification of 2MASS J0320–0446 is so much later than its optical classification (the T dwarf secondary contributes negligible flux in the optical). Figure 8 shows that the 1.3 μm flux increase can be discerned for systems with

early- and mid-type T dwarf companions. While it is again more pronounced for systems with later-type primaries, it is still present (but subtle) in the spectra of systems with M7 primaries. A source with unusually strong absorption at $1.35\ \mu\text{m}$, or equivalently with a near-infrared spectral type that is significantly later than its optical spectral type, may harbor a T dwarf companion. However, other physical effects, notably reduced condensate opacity (e.g., Burgasser et al. 2008), can also give rise to this spectral peculiarity. Hence, both the contrast of the $1.4\ \mu\text{m}$ H_2O band and the presence of the $1.6\ \mu\text{m}$ dip should be considered together as indicators of an unresolved T dwarf companion.

Detecting the near-infrared spectral signature of a T dwarf companion need not be limited to low-resolution observations. While the dip feature at $1.6\ \mu\text{m}$ is less pronounced in the higher-resolution composite spectrum of SCR 1845–6357AB from Kasper et al. (2007), individual CH_4 lines may still be distinguishable amongst the many FeH and H_2O lines present in the same spectral region. It may also be possible to identify CH_4 lines amongst the forest of H_2O lines in the $1.30\text{--}1.35\ \mu\text{m}$ region (e.g. Barber et al. 2006). Such detections require significantly higher resolutions, of order $\lambda/\Delta\lambda \approx 20,000$ or more, due to the substantial overlap of the many molecular features present at these wavelengths (e.g., McLean et al. 2007). Furthermore, an improved line list for the CH_4 molecule may be needed (Sharp & Burrows 2007). Yet such observations have the potential to provide an additional check on the existence and characteristics of mid-type T dwarf companions in binaries with late-M/L dwarf primaries.

Relevant to the identification of late-type M dwarf plus T dwarf binaries from composite near-infrared spectra is the number of such systems that are expected to exist. As a rough estimate, we examined the results of the Monte Carlo mass function and multiplicity simulations presented in Burgasser (2007b). Using the baseline assumptions of these simulations—a mass function that scales as $\frac{dN}{dM} \propto M^{-0.5}$, a component mass range of $0.01 \leq M \leq 0.1\ M_\odot$, a flat age distribution over 10 Gyr, the Baraffe et al. (2003) evolutionary models, and a binary mass ratio distribution that scales as $f(q) \propto q^{1.8}$ (see Allen 2007)—we found that 12–14% of binaries with M8–L0 primaries are predicted to contain a T3–T5 secondary; i.e., detectable with composite near-infrared spectroscopy. These are primarily older systems whose components that just straddle the hydrogen burning minimum mass limit ($\sim 0.07\ M_\odot$; Chabrier & Baraffe 2000). The overall binary fraction of very low mass stars and brown dwarfs has been variously estimated to lie in the 10–35% range (e.g. Bouy et al. 2003; Close et al. 2003; Basri & Reiners 2006; Burgasser et al. 2006b; Burgasser 2007b; Allen 2007; Kraus et al. 2008), and is thus currently uncertain by over a factor of three. However, within this range the Monte Carlo simulations predict that 1–5% of *all* M8–L0 dwarfs harbor a T3–T5 dwarf companion. While this percentage is small, in a given magnitude-limited survey there may be a similar number of T dwarf companions in these relatively bright systems as compared to faint, isolated T dwarfs. Such companions, based on the analysis above, can be reasonably well-characterized without the need of resolved imaging.

There are many other variables that must be considered if the binary spectral template technique described

here and in Burgasser (2007c) is to be used to determine accurate binary statistics for very low mass stars and brown dwarfs. Component peculiarities, such as unusual surface gravities or cloud variations; intrinsic scatter in absolute magnitude/spectral type relations; magnetic- or weather-induced photometric variability; the detailed properties of the still poorly-constrained L dwarf/T dwarf transition; and the possible presence of tertiary components all contribute in constraining the variety of systems that can be identified from composite near-infrared spectroscopy. Furthermore, because brown dwarfs cool over their lifetimes, the detectability of binaries based on component spectral types does not map uniquely to the detectability of binaries based on their mass ratios and ages, resulting in complex selection biases. These issues will be addressed in a future publication.

5. CONCLUSIONS

We have found that subtle peculiarities observed in the near-infrared spectrum of 2MASS J0320–0446, in particular a characteristic bowl-shaped dip at $1.6\ \mu\text{m}$, indicate the presence of a mid-type T dwarf companion. This companion is unresolved in LGS AO imaging observations (including the first application of aperture mask interferometry with LGS AO), indicating a maximum projected separation of 8.3 AU at the time of observations. The binary scenario not only provides a simple and straightforward explanation for the $1.6\ \mu\text{m}$ feature—also present in the composite spectrum of the known M8.5 + T6 binary SCR 1845–6357—but also resolves the discrepancy between the optical and near-infrared classifications of 2MASS J0320–0446. Furthermore, empirical binary templates composed of “normal” M dwarf plus T dwarf pairs provide a far superior match to the overall near-infrared spectral energy distribution of 2MASS J0320–0446 than any single comparison source. The hypothesis that 2MASS J0320–0446 is an unresolved binary is therefore compelling, and could potentially be verified through radial velocity monitoring observations. In addition, we estimate that roughly 1–5% of all late-type M dwarfs may harbor a mid-type T dwarf companion that could similarly be identified and characterized using low resolution near-infrared spectroscopy and binary spectral template analysis.

The authors acknowledge telescope operator Paul Sears and instrument specialist John Rayner at IRTF, and Al Conrad, Randy Campbell, Jason McIlroy, and Gary Punawai at Keck, for their assistance during the observations. We also thank Markus Kasper for providing the spectral data for SCR 1845–6357 and Sandy Leggett, Dagny Looper and Kevin Luhman for providing a portion of the SpeX prism spectra used in the binary spectral template analysis. Our anonymous referee provided a helpful and very prompt critique of the original manuscript. MCL and TJD acknowledge support for this work from NSF grant AST-0507833 and an Alfred P. Sloan Research Fellowship. This publication makes use of data from the Two Micron All Sky Survey, which is a joint project of the University of Massachusetts and the Infrared Processing and Analysis Center, and funded by the National Aeronautics and Space Administration and

the National Science Foundation. 2MASS data were obtained from the NASA/IPAC Infrared Science Archive, which is operated by the Jet Propulsion Laboratory, California Institute of Technology, under contract with the National Aeronautics and Space Administration. This research has benefitted from the M, L, and T dwarf compendium housed at DwarfArchives.org and maintained by Chris Gelino, Davy Kirkpatrick, and Adam Burgasser; the VLM Binaries Archive maintained by Nick Siegler

at <http://www.vlmbinaries.org>; and the SpeX Prism Spectral Libraries, maintained by Adam Burgasser at <http://www.browndwarfs.org/spexprism>. The authors wish to recognize and acknowledge the very significant cultural role and reverence that the summit of Mauna Kea has always had within the indigenous Hawaiian community. We are most fortunate to have the opportunity to conduct observations from this mountain.

Facilities: IRTF (SpeX), Keck (NIRC2,LGS)

REFERENCES

- Abell, G. O. 1959, *PASP*, 67, 258
 Allen, P. R. 2007, *ApJ*, 668, 492
 Allers, K. N., et al. 2007, *ApJ*, 657, 511
 Artigau, É, Doyon, R., Lafrenière, D., Nadeau, D., Robert, J., & Albert, L. 2006, *ApJ*, 651, L57
 Baldwin, J. E., Haniff, C. A., Mackay, C. D., & Warner, P. J. 1986, *Nature*, 320, 595
 Baraffe, I., Chabrier, G., Barman, T., Allard, F., & Hauschildt, P. H. 2003, *A&A*, 382, 563
 Barber, R. J., Tennyson, J., Harris, G. J., & Tolchenov, R. N. 2006, *MNRAS*, 368, 1087
 Basri, G., & Reiners, A. 2006, *AJ*, 132, 663
 Basri, G., & Martín, E. L. 1999, *AJ*, 118, 2460
 Biller, B. A., Kasper, M., Close, L. M., Brandner, W., & Kellner, S. 2006, *ApJ*, 641, L141
 Blake, C. H., Charbonneau, D., White, R. J., Marley, M. S., & Saumon, D. 2007, *ApJ*, 666, 1198
 Bouy, H., Brandner, W., Martín, E. L., Delfosse, X., Allard, F., & Basri, G. 2003, *AJ*, 126, 1526
 Burgasser, A. J. 2007a, *ApJ*, 658, 617
 Burgasser, A. J. 2007b, *ApJ*, 659, 655
 Burgasser, A. J. 2007c, *AJ*, 134, 1330
 Burgasser, A. J., Burrows, A., & Kirkpatrick, J. D. 2006, *ApJ*, 639, 1095
 Burgasser, A. J., Geballe, T. R., Leggett, S. K., Kirkpatrick, J. D., & Golimowski, D. A. 2006a, *ApJ*, 637, 1067
 Burgasser, A. J., Kirkpatrick, J. D., Cruz, K. L., Reid, I. N., Leggett, S. K., Liebert, Burrows, A., & Brown, M. E. 2006b, *ApJS*, 166, 585
 Burgasser, A. J., Kirkpatrick, J. D., Liebert, J., & Burrows, A. 2003a, *ApJ*, 594, 510
 Burgasser, A. J., Kirkpatrick, J. D., McElwain, M. W., Cutri, R. M., Burgasser, A. J., & Skrutskie, M. F. 2003b, *AJ*, 125, 850
 Burgasser, A. J.,Looper, D. L., Kirkpatrick, J. D., & Swift, B. 2008, *ApJ*, in press
 Burgasser, A. J.,Looper, D. L., Kirkpatrick, J. D., & Liu, M. C. 2007a, *ApJ*, 658, 557
 Burgasser, A. J., & McElwain, M. W. 2006, *AJ*, 131, 1007
 Burgasser, A. J., McElwain, M. W., & Kirkpatrick, J. D. 2003, *AJ*, 126, 2487
 Burgasser, A. J., McElwain, M. W., Kirkpatrick, J. D., Cruz, K. L., Tinney, C. G., & Reid, I. N. 2004b, *AJ*, 127, 2856
 Burgasser, A. J., Reid, I. N., Leggett, S. J., Kirkpatrick, J. D., Liebert, J., & Burrows, A. 2005, *ApJ*, 634, L177
 Burgasser, A. J., Reid, I. N., Siegler, N., Close, L. M., Allen, P., Lowrance, P. J., & Gizis, J. E. 2007b, in *Planets and Protostars V*, eds. B. Reipurth, D. Jewitt and K. Keil (Univ. Arizona Press: Tucson), p. 427
 Burgasser, A. J., et al. 1999, *ApJ*, 522, L65
 Burgasser, A. J., et al. 2000a, *ApJ*, 531, L57
 Burgasser, A. J., et al. 2000b, *AJ*, 120, 1100
 Burgasser, A. J., et al. 2002, *ApJ*, 564, 421
 Burrows, A., et al. 1997, *ApJ*, 491, 856
 Chabrier, G., & Baraffe, I. 2000, *ARA&A*, 38, 337
 Chauvin, G., Lagrange, A.-M., Dumas, C., Zuckerman, B., Mouillet, D., Song, I., Beuzit, J.-L., & Lowrance, P. 2004, *A&A*, 425, L29
 Chiu, K., Fan, X., Leggett, S. K., Golimowski, D. A., Zheng, W., Geballe, T. R., Schneider, D. P., & Brinkmann, J. 2006, *AJ*, 131, 2722
 Close, L. M., Siegler, N., Freed, M., & Biller, B. 2003, *ApJ*, 587, 407
 Cruz, K. L., Burgasser, A. J., Reid, I. N., & Liebert, J. 2004, 604, L61
 Cruz, K. L., Reid, I. N., Liebert, J., Kirkpatrick, J. D., & Lowrance, P. J. 2003, *AJ*, 126, 2421
 Cruz, K. L., et al. 2007, *AJ*, 133, 439
 Cushing, M. C., Rayner, J. T., Davis, S. P., & Vacca, W. D. 2003, *ApJ*, 582, 1066
 Cushing, M. C., Vacca, W. D., & Rayner, J. T. 2004, *PASP*, 116, 362
 Deacon, N. R., Hambly, N. C., & Cooke, J. A. 2005, *A&A*, 435, 363
 Ellis, S. C., Tinney, C. G., Burgasser, A. J., Kirkpatrick, J. D., & McElwain, M. W. 2005, *AJ*, 130, 2347
 Folkes, S. L., Pinfield, D. J., Kendall, T. R., & Jones, H. R. A. 2007, *MNRAS*, 378, 901
 Geballe, T. R., et al. 2002, *ApJ*, 564, 466
 Gelino, C. R., Kulkarni, S. R., & Stephens, D. C. 2006, *PASP*, 118, 611
 Gizis, J. E. 2002, *ApJ*, 575, 484
 Gizis, J. E., Kirkpatrick, J. D., & Wilson, J. C. 2001, *AJ*, 121, 2185
 Gizis, J. E., Monet, D. G., Reid, I. N., Kirkpatrick, J. D., Liebert, J., & Williams, R. 2000, *AJ*, 120, 1085
 Golimowski, D. A., et al. 2004, *AJ*, 127, 3516
 Gorlova, N. I., Meyer, M. R., Rieke, G. H., & Liebert, J. 2003, *ApJ*, 593, 1074
 Hambly, N. C., Davenhall, A. C., Irwin, M. J., & MacGillivray, H. T. 2001a, *MNRAS* 326, 1315
 Hambly, N. C., Henry, T. J., Subasavage, J. P., Brown, M. A., & Jao, W.-C. 2004, *AJ*, 128, 473
 Hambly, N. C., Irwin, M. J., & MacGillivray, H. T. 2001b, *MNRAS* 326, 1295
 Hambly, N. C., MacGillivray, H. T., Read, M. A., et al. 2001c, *MNRAS* 326, 1279
 Hawley, S. L. et al. 2002, *AJ*, 123, 3409
 Henry, T. J., Jao, W.-C., Subasavage, J. P., Beaulieu, T. D., Ianna, P. A., Costa, E., & Méndez, R. A. 2006, *AJ*, 132, 2360
 Ireland, M. J., Kraus, A., Martinache, F., Lloyd, J. P., & Tuthill, P. G. 2008, *ApJ*, in press
 Joergens, V., & Müller, A. 2007, *ApJ*, 666, L113
 Kasper, M., Biller, B. A., Burrows, A., Brandner, W., Budaj, J., & Close, L. M. 2007, *A&A*, 471, 655
 Kendall, T. R., Delfosse, X., Martín, E. L., & Forveille, T. 2004, *A&A*, 416, L17
 Kenyon, M. J., Jeffries, R. D., Naylor, T., Oliveira, J. M., & Maxted, P. F. L. 2005, *MNRAS*, 356, 89
 Kirkpatrick, J. D. 2005, *ARA&A*, 43, 195
 Kirkpatrick, J. D. Barman, T. S., Burgasser, A. J., McGovern, M. R., McLean, I. S., Tinney, C. G., & Lowrance, P. J. 2006, *ApJ*, 639, 1120
 Kirkpatrick, J. D., Beichman, C. A., & Skrutskie, M. F. 1997, *ApJ*, 476, 311
 Kirkpatrick, J. D., Henry, T. J., & McCarthy, D. W., Jr. 1991, *ApJS*, 77, 417
 Kirkpatrick, J. D., Reid, I. N., Liebert, J., Gizis, J. E., Burgasser, A. J., Monet, D. G., Dahn, C. C., Nelson, B., & Williams, R. J. 2000, *AJ*, 120, 447
 Kirkpatrick, J. D., et al. 1999, *ApJ*, 519, 802
 Knapp, G., et al. 2004, *ApJ*, 127, 3553
 Kraus, A. L., Ireland, M. J., Martinache, F., & Lloyd, J. P. 2008, *ApJ*, in press
 Kraus, A. L., White, R. J., & Hillenbrand, L. A. 2005, *ApJ*, 633, 452
 Lane, B. F., Zapatero Osorio, M. R., Britton, M. C., Martín, E. L., & Kulkarni, S. R. 2001, *ApJ*, 560, 390
 Leggett, S. K., Marley, M. S., Freedman, R., Saumon, D., Liu, M. C., Geballe, T. R., Golimowski, D. A., & Stephens, D. 2007, *ApJ*, 667, 537

- Leggett, S. K., et al. 2000b, *ApJ*, 536, L35
- Liebert, J., & Burgasser, A. J. 2007, *ApJ*, 655, 522
- Liebert, J., & Gizis, J. E. 2006, *PASP*, 118, 659
- Liebert, J., Kirkpatrick, J. D., Cruz, K. L., Reid, I. N., Burgasser, A. J., Tinney, C. G., & Gizis, J. E. 2003, *AJ*, 125, 343
- Liu, M. C., Dupuy, T. J., & Ireland, M. J. 2008, *ApJ*, submitted
- Liu, M. C., & Leggett, S. K. 2005, *ApJ*, 634, 616
- Liu, M. C., Leggett, S. K., & Chiu, K. 2007, *ApJ*, 660, 1507
- Liu, M. C., Leggett, S. K., Golimowski, D. A., Chiu, K., Fan, X., Geballe, T. R., Schneider, D. P., & Brinkmann, J. 2006, *ApJ*, 647, 1393
- Lodieu, N., Scholz, R.-D., McCaughrean, M. J., Ibata, R., Irwin, M., & Zinnecker, H. 2005, *A&A*, 440, 1061
- Looper, D. L., Kirkpatrick, J. D., & Burgasser, A. J. 2007, *AJ*, 134, 1162
- Looper, D. L., Liu, M. C., Gelino, C. R., Burgasser, A. J., & Kirkpatrick, J. D. 2008, *ApJ*, submitted
- Luhman, K. L., Joergens, V., Lada, C., Muzerolle, J., Pascucci, I., & White, R. 2007a, in *Planets and Protostars V*, eds. B. Reipurth, D. Jewitt and K. Keil (Univ. Arizona Press: Tucson), p. 443
- Luhman, K. L., & Rieke, G. H. 1999, *ApJ*, 525, 440
- Luhman, K. L., et al. 2007b, *ApJ*, 654, 570
- Martín, E. L., Brandner, W., & Basri, G. 1999, *Science*, 283, 1718
- Martín, E. L., Brandner, W., Bouy, H., Basri, G., Davis, J., Deshpande, R., Montgomery, M., & King, I. 2006, *A&A*, 456, 253
- Martín, E. L., Delfosse, X., Basri, G., Goldman, B., Forveille, T., & Zapatero Osorio, M. R. 1999, *AJ*, 118, 2466
- McElwain, M. W., & Burgasser, A. J. 2006, *AJ*, 132, 2074
- McLean, I. S., McGovern, M. R., Burgasser, A. J., Kirkpatrick, J. D., Prato, L., & Kim, S. 2003, *ApJ*, 596, 561
- McLean, I. S., Prato, L., McGovern, M. R., Burgasser, A. J., Kirkpatrick, J. D., Rice, E. L., & Kim, S. S. 2007, *ApJ*, 658, 1217
- Michelson, A. A. 1920, *ApJ*, 51, 257
- Monet, D. G., et al. 2003, *AJ*, 125, 984 (USNO-B1.0 Catalog)
- Montagnier, G., et al. 2006, *A&A*, 460, L19
- Mugrauer, M., Seifahrt, A., Neuhauser, R., & Mazeh, T. 2006, *MNRAS*, 373, L31
- Nakajima, T., Kulkarni, S. R., Gorham, P. W., Ghez, A. M., Neugebauer, G., Oke, J. B., Prince, T. A., & Readhead, A. C. S. 1989, *AJ*, 97, 1510
- Pokorny, R. S., Jones, H. R. A., Hambly, N. C., & Pinfield, D. J. 2004, *A&A*, 421, 763
- Pravdo, S. H., Shaklan, S. B., Wiktorowicz, S. J., Kulkarni, S., Lloyd, J. P., Martinache, F., Tuthill, P. G., & Ireland, M. J. 2006, *ApJ*, 649, 389
- Rayner, J. T., Toomey, D. W., Onaka, P. M., Denault, A. J., Stahlberger, W. E., Vacca, W. D., Cushing, M. C., & Wang, S. 2003, *PASP*, 155, 362
- Reid, I. N., Burgasser, A. J., Cruz, K. L., Kirkpatrick, & J. D., Gizis 2001, *AJ*, 121, 1710
- Reid, I. N., Kirkpatrick, J. D., Gizis, J. E., Dahn, C. C., Monet, D. G., Williams, R. J., Liebert, J., & Burgasser, A. J. 2000, *AJ*, 119, 369
- Reid, I. N., Lewitus, E., Allen, P. R., Cruz, K. L., & Burgasser, A. J. 2006a, *AJ*, 132, 891
- Reid, I. N., Lewitus, E., Cruz, K. L., & Burgasser, A. J. 2006b, *ApJ*, 639, 1114
- Ruiz, M. T., & Takamiya, M. Y. 1995, *AJ*, 109, 2817
- Scholz, R.-D., & Meusinger, H. 2002, *MNRAS*, 336, L49
- Sharp, C. M., & Burrows, A. 2007, *ApJS*, 168, 140
- Siegler, N., Close, L. M., Mamajek, E. E., & Freed, M. 2003, *ApJ*, 598, 1265
- Siegler, N., Close, L. M., Cruz, K. L., Martín, E. L., & Reid, I. N. 2005, *ApJ*, 621, 1023
- Siegler, N., Close, L. M., Burgasser, A. J., Cruz, K. L., Macintosh, B., Marios, C., & Barman, T. 2007, *AJ*, 133, 2320
- Simons, D. A., & Tokunaga, A. T. 2002, *PASP*, 114, 169
- Skrutskie, M. F., et al. 2006, *AJ*, 131, 1163
- Stassun, K., Mathieu, R. D., Vaz, L. P. R., Valenti, J. A., & Gomez, Y. 2006, *Nature*, 440, 311
- Strauss, M. A., et al. 1999, *ApJ*, 522, L61
- Stephens, D. C., & Leggett, S. K. 2004, *PASP*, 116, 9
- Teegarden, B. J., et al. 2003, *ApJ*, 589, L51
- Tinney, C. G., Burgasser, A. J., Kirkpatrick, J. D., & McElwain, M. W. 2005, *AJ*, 130, 2326
- Tokunaga, A. T., & Kobayashi, N. 1999, *AJ*, 117, 1010
- Tokunaga, A. T., Simons, D. A., & Vacca W. D. 2002, *PASP*, 114, 180
- Tsvetanov, Z. I., et al. 2000, *ApJ*, 531, L61
- Tuthill, P. G., Monnier, J. D., Danchi, W. C., Wishnow, E. H., & Haniff, C. A. 2000, *PASP*, 112, 555
- Vacca, W. D., Cushing, M. C., & Rayner, J. T. 2003, *PASP*, 155, 389
- van Biesbroeck, G. 1961, *AJ*, 66, 528
- van Dam, M. A., et al. 2006, *PASP*, 118, 310
- Vrba, F. J., et al. 2004, *AJ*, 127, 2948
- Wallace, L., & Hinkle, K. 2001, *ApJ*, 559, 424
- Wilson, J. C., Miller, N. A., Gizis, J. E., Skrutskie, M. F., Houck, J. R., Kirkpatrick, J. D., Burgasser, A. J., & Monet, D. G. 2003, in *Brown Dwarfs (IAU Symp. 211)*, ed. E. Martín (San Francisco: ASP), p. 197
- Wilson, J. C., et al. 2001b, *AJ*, 122, 1989
- Wizinowich, P. L., et al. 2006, *PASP*, 118, 297
- Zapatero Osorio, M. R., Lane, B. F., Pavlenko, Ya., Martín, E. L., Britton, M., & Kulkarni, S. R. 2004, *ApJ*, 615, 958

TABLE 1
 SPEX SPECTRAL TEMPLATES.

Name	2MASS Designation ^a	Spectral Types		2MASS <i>J</i>	References ^b
		Optical	NIR		
SDSS J0000+2554	J00001354+2554180	...	T4.5	15.06±0.04	1;2
2MASS J0034+0523	J00345157+0523050	...	T6.5	15.54±0.05	3;1
2MASS J0036+1821	J00361617+1821104	L3.5	L4±1	12.47±0.03	4;2,5,6
HD 3651B	J0039191+211516	...	T7.5	16.16±0.03	7;8,9,10
2MASS J0050-3322	J00501994-3322402	...	T7	15.93±0.07	11;1,12
2MASS J0103+1935	J01033203+1935361	L6	...	16.29±0.08	13;6
2MASS J0117-3403	J01174748-3403258	L2:	...	15.18±0.04	56;14
SDSS J0119+2403	J01191207+2403317	...	T2	17.02±0.18	15
IPMS 0136+0933	J01365662+0933473	...	T2.5	13.46±0.03	4;16
2MASS J0144-0716	J01443536-0716142	L5	...	14.19±0.03	4;17
SDSS J0151+1244	J01514155+1244300	...	T1	16.57±0.13	3;1,18
2MASS J0205+1251	J02050344+1251422	L5	...	15.68±0.06	19;6
SDSS J0207+0000	J02074284+0000564	...	T4.5	16.80±0.16	1;18
2MASS J0208+2542	J02081833+2542533	L1	...	13.99±0.03	4;6
SIPS J0227-1624	J02271036-1624479	L1	...	13.57±0.02	4;20
2MASS J0228+2537	J02281101+2537380	L0:	L0	13.84±0.03	4;14,21
GJ 1048B	J02355993-2331205	L1	L1	...	4;22
2MASS J0241-1241	J02415367-1241069	L2:	...	15.61±0.07	56;14
2MASS J0243-2453	J02431371-2453298	...	T6	15.38±0.05	3;1,23
SDSS J0247-1631	J02474978-1631132	...	T2±1.5	17.19±0.18	15
SO 0253+1625	J02530084+1652532	M7	...	8.39±0.03	4;24,25
DENIS J0255-4700	J02550357-4700509	L8	L9	13.25±0.03	1;26,27
2MASS J0310+1648	J03105986+1648155	L8	L9	16.03±0.08	28;1,6
SDSS J0325+0425	J03255322+0425406	...	T5.5	16.25±0.14	15
2MASS J0328+2302	J03284265+2302051	L8	L9.5	16.69±0.14	4;2,6
LP 944-20	J03393521-3525440	M9	...	10.73±0.02	4
2MASS J0345+2540	J03454316+2540233	L0	L1±1	14.00±0.03	29;2,30,31
SDSS J0351+4810	J03510423+4810477	...	T1±1.5	16.47±0.13	15
2MASS J0407+1514	J04070885+1514565	...	T5	16.06±0.09	3;1
2MASS J0415-0935	J04151954-0935066	T8	T8	15.70±0.06	3;1,23,32
2MASS J0439-2353	J04390101-2353083	L6.5	...	14.41±0.03	28;14
2MASS J0510-4208	J05103520-4208140	...	T5	16.22±0.09	33
2MASS J0516-0445	J05160945-0445499	...	T5.5	15.98±0.08	4;1,34
2MASS J0559-1404	J05591914-1404488	T5	T4.5	13.80±0.02	1;32,35
2MASS J0602+4043	J06020638+4043588	...	T4.5	15.54±0.07	33
LEHPM 2-461	J06590991-4746532	M6.5	M7	13.64±0.03	4;36,37
2MASS J0727+1710	J07271824+1710012	T8	T7	15.60±0.06	11;23,32
2MASS J0729-3954	J07290002-3954043	...	T8	15.92±0.08	33
2MASS J0755+2212	J07554795+2212169	T6	T5	15.73±0.06	1;23,32
SDSS J0758+3247	J07584037+3247245	...	T2	14.95±0.04	4;1,2
SSSPM 0829-1309	J08283419-1309198	L2	...	12.80±0.03	38;39,40
SDSS J0830+4828	J08300825+4828482	L8	L9±1	15.44±0.05	4;18,27
SDSS J0837-0000	J08371718-0000179	T0±2	T1	17.10±0.21	33;1,32,41
2MASS J0847-1532	J08472872-1532372	L2	...	13.51±0.03	42;14
SDSS J0858+3256	J08583467+3256275	...	T1	16.45±0.12	15
SDSS J0909+6525	J09090085+6525275	...	T1.5	16.03±0.09	15
2MASS J0939-2448	J09393548-2448279	...	T8	15.98±0.11	1;12
2MASS J0949-1545	J09490860-1545485	...	T2	16.15±0.12	1;12
2MASS J1007-4555	J10073369-4555147	...	T5	15.65±0.07	33
2MASS J1010-0406	J10101480-0406499	L6	...	15.51±0.06	19
HD 89744B	J10221489+4114266	L0	L (early)	14.90±0.04	4;43
SDSS J1039+3256	J10393137+3256263	...	T1	16.41±0.15	15
2MASS J1047+2124	J10475385+2124234	T7	T6.5	15.82±0.06	4;1,32,44
SDSS J1048+0111	J10484281+0111580	L1	L4	12.92±0.02	4;45,46
SDSS J1052+4422	J10521350+4422559	...	T0.5±1	15.96±0.10	4;15
Wolf 359	J10562886+0700527	M6	...	7.09±0.02	4
2MASS J1104+1959	J11040127+1959217	L4	...	14.38±0.03	3;14
2MASS J1106+2754	J11061197+2754225	...	T2.5	14.82±0.04	33
SDSS J1110+0116	J11101001+0116130	...	T5.5	16.34±0.12	11;1,18
2MASS J1114-2618	J11145133-2618235	...	T7.5	15.86±0.08	11;1,12
2MASS J1122-3512	J11220826-3512363	...	T2	15.02±0.04	1;12
2MASS J1124+3808	J11240487+3808054	M8.5	...	12.71±0.02	3;14
SDSS J1206+2813	J12060248+2813293	...	T3	16.54±0.11	15
SDSS J1207+0244	J12074717+0244249	L8	T0	15.58±0.07	33;1,45
2MASS J1209-1004	J12095613-1004008	...	T3	15.91±0.07	3;1,27
SDSS J1214+6316	J12144089+6316434	...	T3.5±1	16.59±0.12	15
2MASS J1217-0311	J12171110-0311131	T7	T7.5	15.86±0.06	11;1,32,44
2MASS J1221+0257	J12212770+0257198	L0	...	13.17±0.02	4;47
2MASS J1231+0847	J12314753+0847331	...	T5.5	15.57±0.07	3;1
2MASS J1237+6526	J12373919+6526148	T7	T6.5	16.05±0.09	48;1,32,44
SDSS J1254-0122	J12545393-0122474	T2	T2	14.89±0.04	3;1,32,44
2MASS J1324+6358	J13243559+6358284	...	T2	15.60±0.07	33
SDSS J1346-0031	J13464634-0031501	T7	T6.5	16.00±0.10	11;1,32,49
SDSS J1358+3747	J13585269+3747137	...	T4.5±1	16.46±0.09	15
2MASS J1404-3159	J14044941-3159329	...	T2.5	15.60±0.06	33
LHS 2924	J14284323+3310391	M9	...	11.99±0.02	29
SDSS J1435+1129	J14355323+1129485	...	T2±1	17.14±0.23	15
2MASS J1439+1020	J14393836+1020149	L1	...	12.76±0.02	3;21

TABLE 2
 PREDICTED COMPONENT PARAMETERS FOR 2MASS J0320–0446.

Parameter	2MASS J0320–0446A	2MASS J0320–0446B	Difference
Spectral Type	M8.5±0.3	T5±0.9	...
J^a (mag)	13.25±0.03	16.4±0.4	3.1±0.4
H^a (mag)	12.61±0.03	16.4±0.5	3.8±0.5
K^a (mag)	12.13±0.03	16.5±0.6	4.3±0.6
$\log_{10} L_{bol}/L_{\odot}^b$	-3.48±0.10	-5.0±0.3	1.5±0.3
μ ($''$ yr $^{-1}$)	0.562±0.005
ϕ ($^{\circ}$)	205.9±0.5
d^c (pc)	25±3
V_{tan} (km s $^{-1}$)	67±8
ρ (AU)	<8.3 (<0 $'$ 33)
Mass (M_{\odot}) at 1 Gyr d	0.081	0.035	0.44 e
Mass (M_{\odot}) at 5 Gyr d	0.086	0.068	0.79 e
Mass (M_{\odot}) at 10 Gyr d	0.086	0.074	0.86 e

^aSynthetic magnitudes on the MKO system, based on 2MASS JHK_s photometry for the unresolved source and binary template fits using the “bright” M_K /spectral type relation of Liu et al. (2006).

^bBased on the M_{bol} /spectral type relation of Burgasser (2007b).

^cBased on the inferred J magnitude and spectral type of the primary, and the M_J /spectral type relation of Cruz et al. (2003).

^dBased on evolutionary models from Burrows et al. (1997) and the estimated luminosities.

^eMass ratio $q \equiv M_2/M_1$.

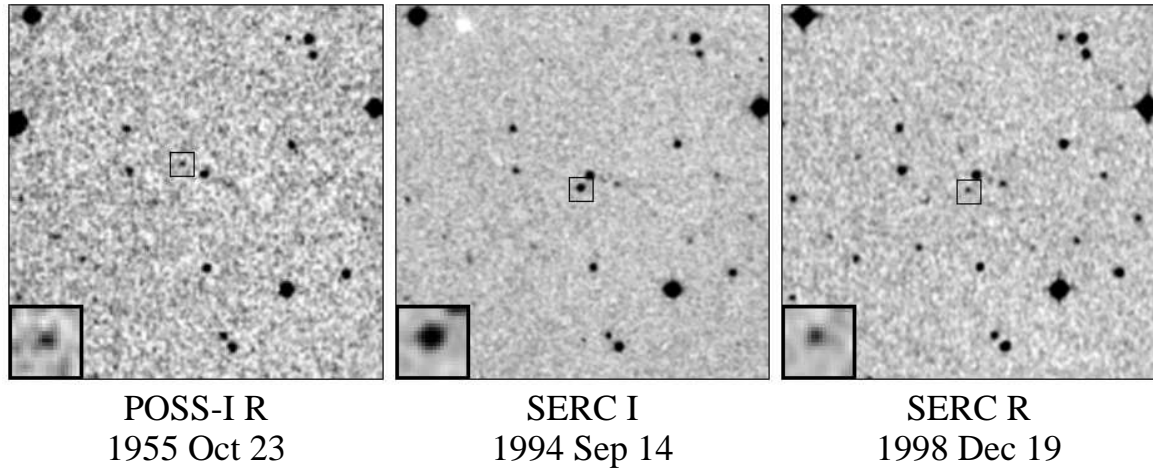


FIG. 1.— Field images of 2MASS J0320–0446 from ESO *R* (left), SERC I_N (middle) and SERC *R* (right) photographic plates. All images are scaled to the same spatial resolution, are $5'$ on a side, and are oriented with north up and east to the left. Inset boxes $20'' \times 20''$ in size indicate the position of the source after correcting for its motion ($\mu = 0''.562 \pm 0''.005 \text{ yr}^{-1}$ at position angle $\theta = 205^\circ.9 \pm 0^\circ.5$) and are expanded in the lower left corner of each image.

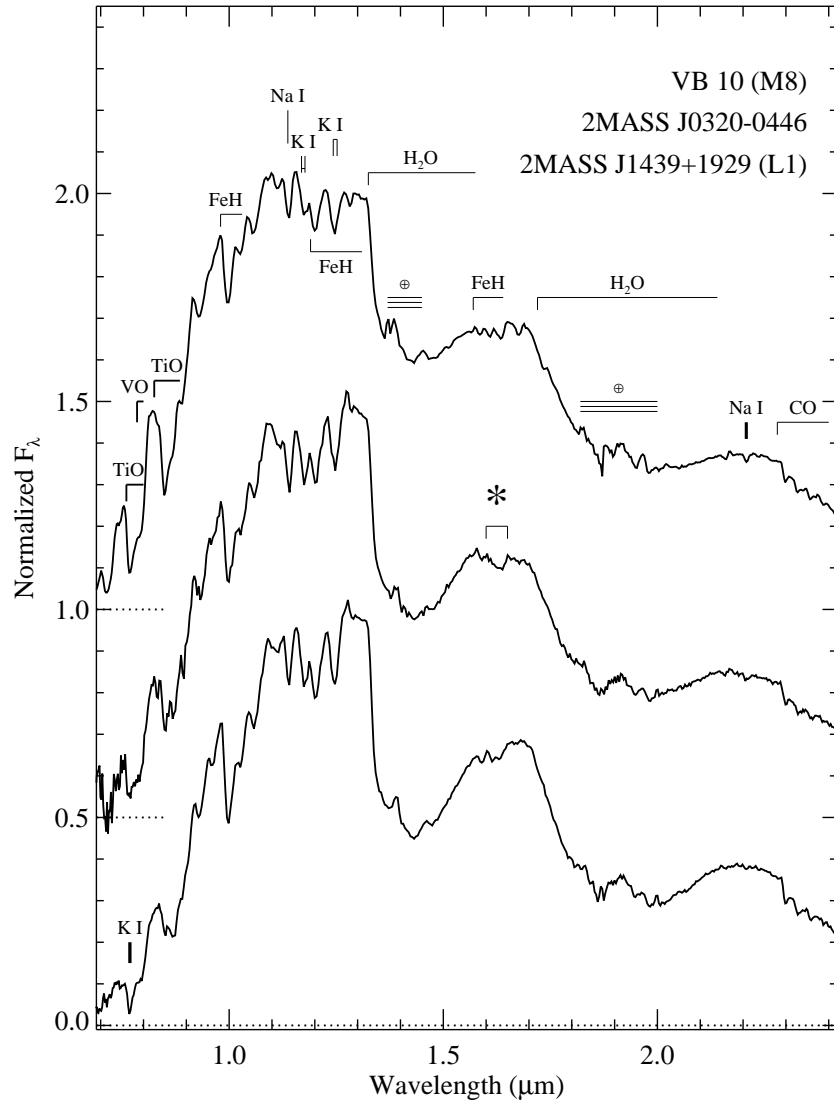


FIG. 2.— SpeX prism spectrum for 2MASS J0320-0446 (center) compared to equivalent data for VB 10 (M8) and 2MASS J1439+1929 (L1; see Table 1). Spectra are normalized at $1.25 \mu\text{m}$ and offset by constants (dotted lines). Prominent features resolved by these spectra are indicated. The peculiar $1.6 \mu\text{m}$ feature in the spectrum of 2MASS J0320-0446 discussed in the text is indicated by an asterisk.

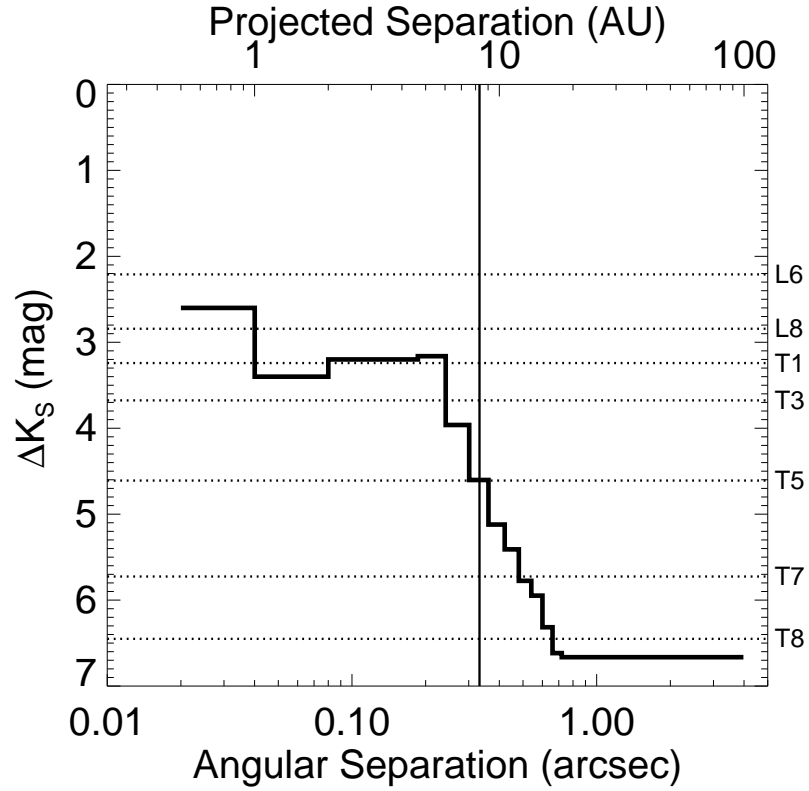


FIG. 3.— Upper limits on the relative K_s -band flux ratio of a faint companion to 2MASS J0320–0446 as a function of separation based on LGS AO observations. The limits shortward of $0''.25$ are based on observations with a 9-hole, non-redundant aperture mask, while those longward are based on direct imaging observations. Angular separation in arcseconds is mapped onto projected separation in AU at the estimated distance of 25 pc. Flux ratios are mapped onto secondary spectral type using the “bright” MKO M_K /spectral type relation of Liu et al. (2006) and spectral type-dependent filter transformations from Stephens & Leggett (2004).

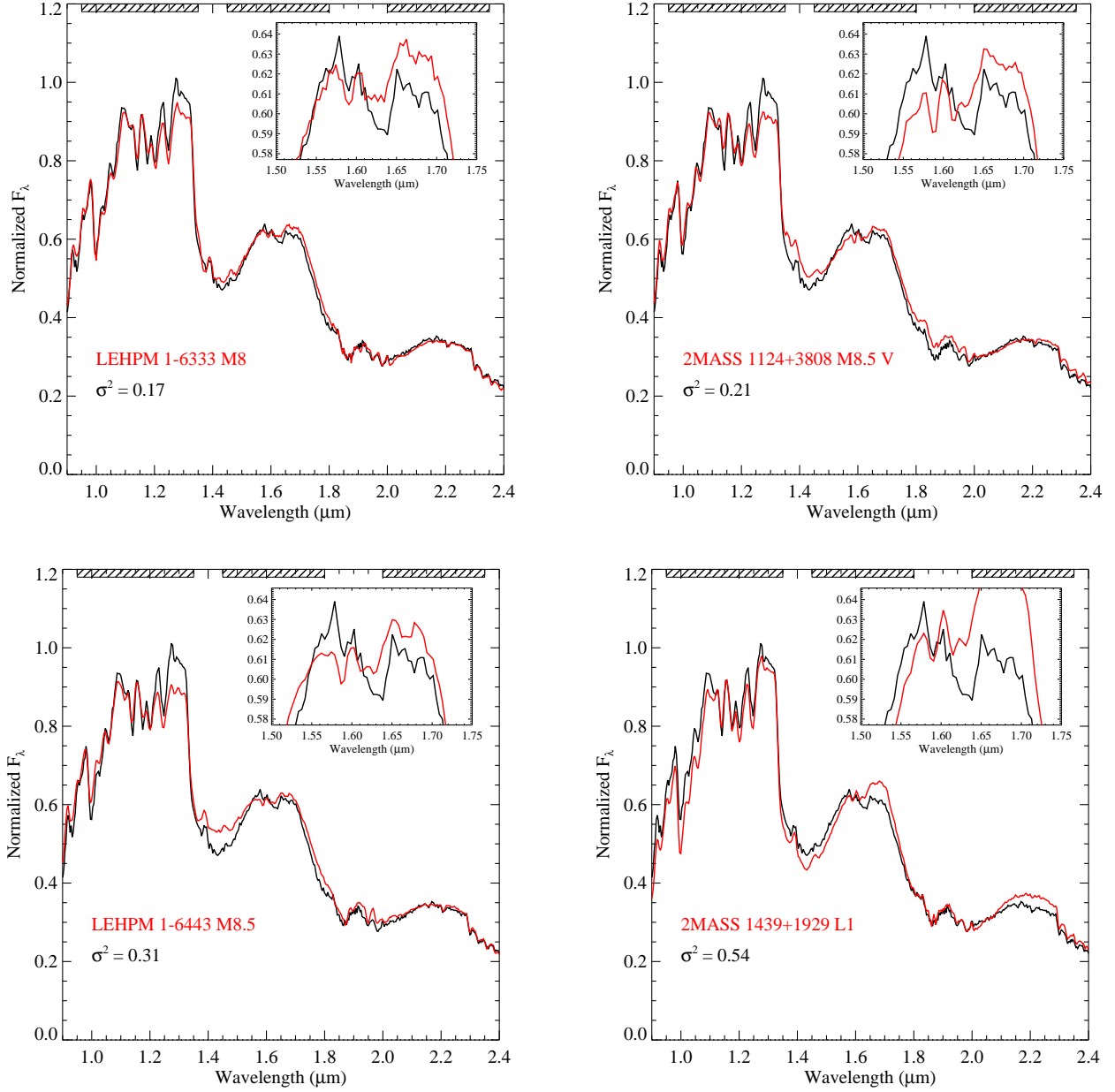


FIG. 4.— Best fit single spectral templates (red lines) to the spectrum of 2MASS J0320–0446 (black lines): LEHPM 1-6333 (M8, $\sigma^2 = 0.17$), 2MASS J1124+3808 (M8.5, $\sigma^2 = 0.21$), LEHPM 1-6443 (M8.5, $\sigma^2 = 0.31$) and 2MASS J1439+1929 (L1, $\sigma^2 = 0.54$). All spectra are normalized in the 1.2–1.3 μm window, with the templates further scaled to minimize their σ^2 deviations. The spectral bands used to calculate σ^2 are indicated at the top of each panel. Inset boxes show a close-up of the 1.5–1.75 μm region where the peculiar 1.6 μm feature present in the spectrum of 2MASS J0320–0446 is located.

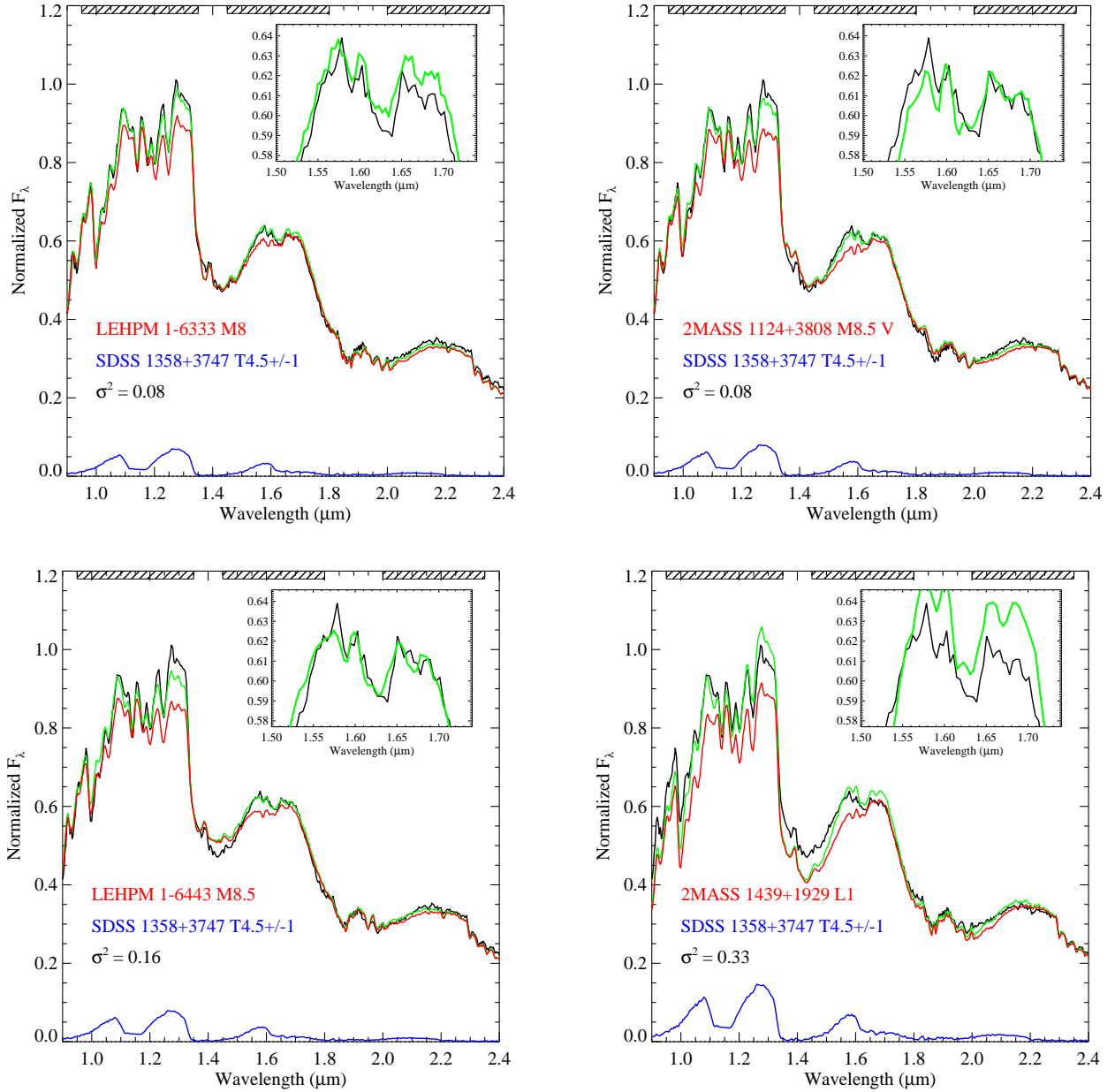


FIG. 5.— Best fit binary spectral templates (green lines) to the spectrum of 2MASS J0320-0446 (black lines) constructed from the primaries shown in Figure 4 and using the “faint” M_K /spectral type relation of Liu et al. (2006). The primary (red lines) and secondary (blue lines) component spectra are shown scaled in accordance with their contribution to the binary templates. Inset boxes show a close-up of the 1.5–1.75 μm spectra of 2MASS J0320-0446 and binary templates.

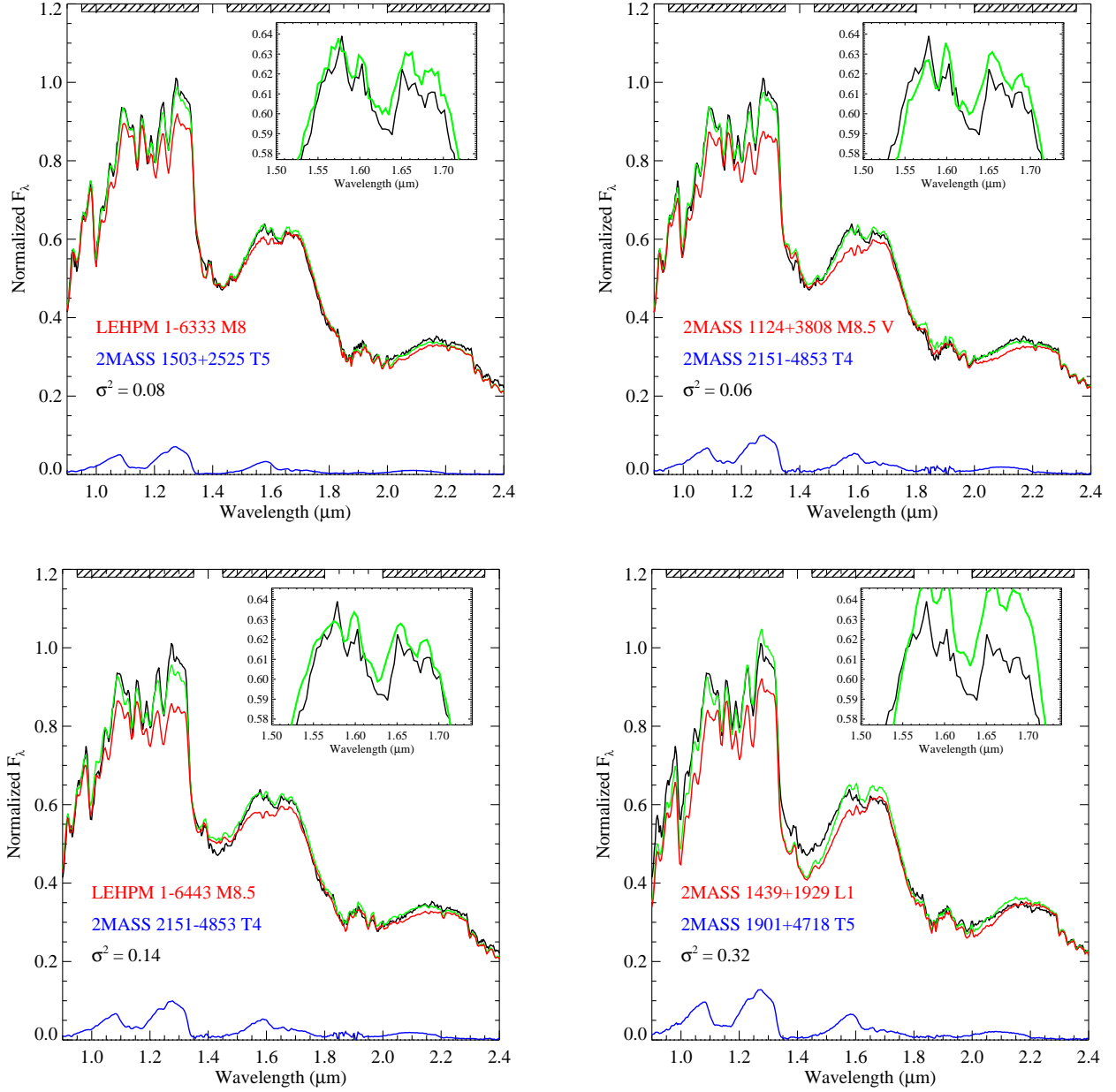


FIG. 6.— Same as Figure 6 but based on binary spectral templates constructed using the “bright” M_K /spectral type relation of Liu et al. (2006).

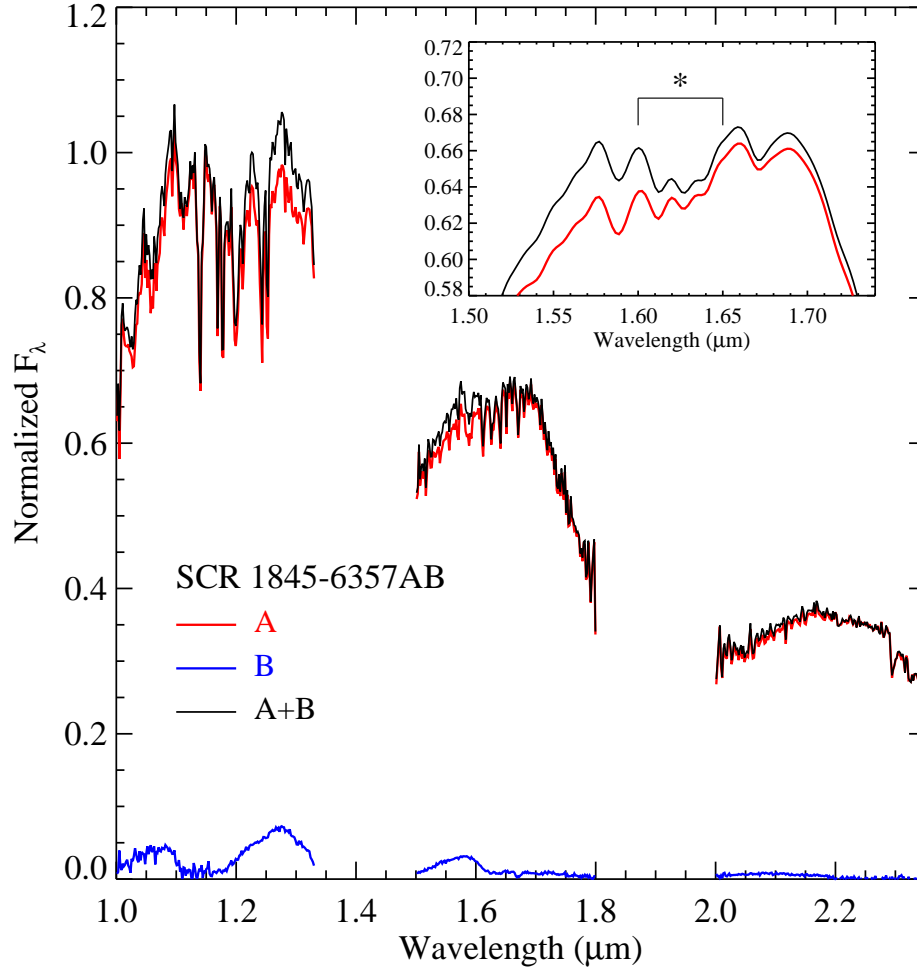


FIG. 7.— Component spectra of SCR 1845–6357AB from Kasper et al. (2007). The M8.5 primary (red lines) and T6 secondary (blue lines) spectra are scaled according to the relative H -band component photometry as reported by Kasper et al. The sum of the component spectra (black lines) shows a slight increase in both 1.25–1.35 μm and 1.55–1.6 μm flux. The inset box shows a close-up of the primary and composite spectra in the 1.5–1.75 μm region, where their spectral resolutions have been reduced to match that of the SpeX prism data. A weak 1.6 μm dip, similar to that seen in the spectrum of 2MASS J0320–0446, is also found to be present in the composite SCR 1845–6357 spectrum.

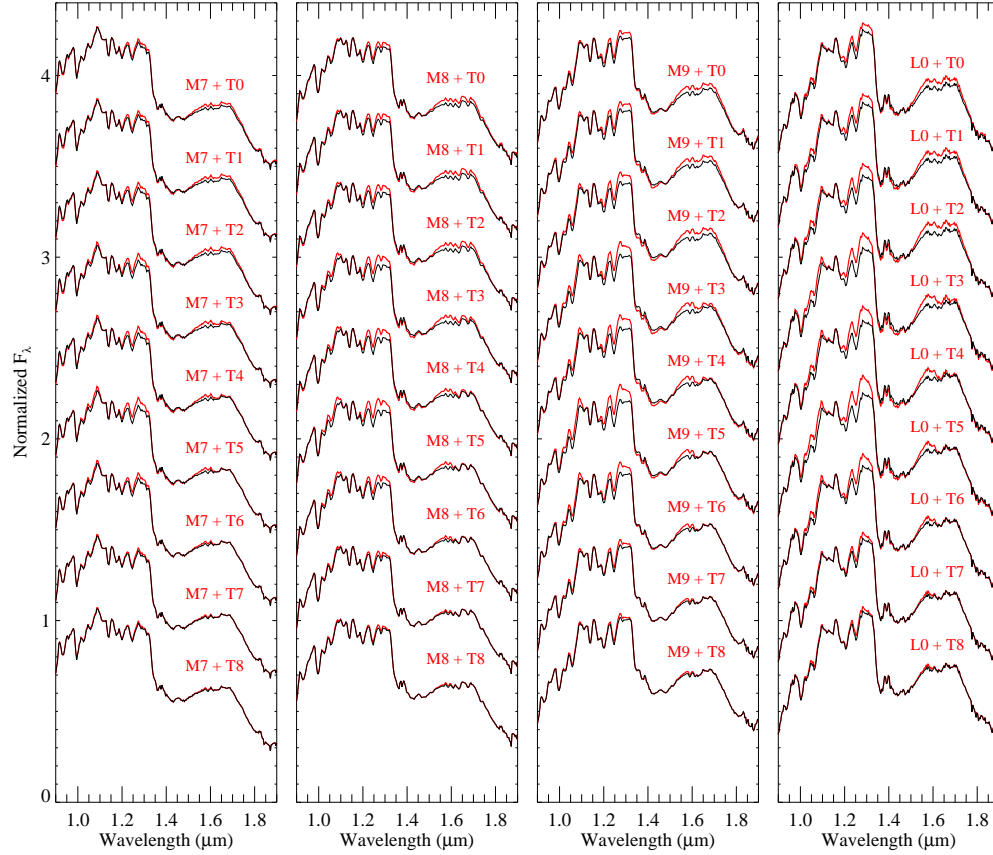


FIG. 8.— Simulated M7–L0 plus T dwarf binary spectra (red lines), based on the “bright” M_K /spectral type relation of Liu et al. (2006). The primaries shown (black lines) are VB 8 (M7), VB 10 (M8), LHS 2924 (M9) and 2MASS J0345+2540 (L0; see Table 1). The T dwarf secondaries are the standards defined in Burgasser et al. (2006a). Binary templates were constructed as described in § 3.3, and all spectra are normalized in the 1.12–1.17 μm region where the T dwarf companions contribute minimal flux.